

Simulation of relativistically colliding laser-generated electron flows

X. H. Yang,^{1,2} M. E. Dieckmann,^{1,*} G. Sarri,¹ and M. Borghesi^{1,3}

¹*Centre for Plasma Physics, School of Mathematics and Physics,
Queen's University of Belfast, Belfast BT7 1NN, United Kingdom*

²*College of Science, National University of Defense Technology, Changsha 410073, China*

³*Institute of Physics of the ASCR, ELI-Beamlines project, Na Slovance 2, 18221 Prague, Czech Republic*
(Dated: September 16, 2021)

The plasma dynamics resulting from the simultaneous impact, of two equal, ultra-intense laser pulses, in two spatially separated spots, onto a dense target is studied via particle-in-cell (PIC) simulations. The simulations show that electrons accelerated to relativistic speeds, cross the target and exit at its rear surface. Most energetic electrons are bound to the rear surface by the ambipolar electric field and expand along it. Their current is closed by a return current in the target, and this current configuration generates strong surface magnetic fields. The two electron sheaths collide at the midplane between the laser impact points. The magnetic repulsion between the counter-streaming electron beams separates them along the surface normal direction, before they can thermalize through other beam instabilities. This magnetic repulsion is also the driving mechanism for the beam-Weibel (filamentation) instability, which is thought to be responsible for magnetic field growth close to the internal shocks of gamma-ray burst (GRB) jets. The relative strength of this repulsion compared to the competing electrostatic interactions, which is evidenced by the simulations, suggests that the filamentation instability can be examined in an experimental setting.

PACS numbers: 52.38Kd, 52.38.Fz, 52.65.Rr

I. INTRODUCTION

The dynamics of the transient electromagnetic field driven by relativistic electronic surface currents, which are generated by the interaction of ultra-intense laser beams with solids [1–3], are of relevance to important applications such as laser-driven ion acceleration [4, 5] and fast ignition [6]. The surface magnetic and electrostatic fields can be of the order of $\sim 10^3\text{T}$ and $\sim 10^{12}\text{V/m}$ [7–9], respectively, during the ultra-intense ($I > 10^{19}\text{W/cm}^2$) laser-solid interaction, and such fields can last several tens of picoseconds after the laser pulse ends. Charging of a laser-irradiated target, which is attributed to the escape of hot electrons generated during the laser-plasma interaction, has been detected in several experiments [10, 11] using proton probing techniques. Because of their confinement by the sheath electric field and surface magnetic field, most of the hot electrons are bound to the target surface [3, 12–14] as they move away from the interaction region. The surface current is closed by the return current within the target and this current loop encloses a strong magnetic field. This magnetic field generation mechanism is known as the fountain effect. Recent experiments [15, 16] have demonstrated that, during the ultra-intense laser irradiating the target, the magnetic field tied to the electron current expands along the solid's surface at a speed close to that of light.

If two ultra-intense laser pulses of comparable intensity irradiate the target's surface at two separate points si-

multaneously, they produce two relativistic electron flows at the rear surface. Both flows collide head-on half-way between the two interaction points at the planar rear surface. The superposition of their respective currents, which are oppositely directed and comparable in magnitude, initially results in a net current density, which is low compared to the current density of each electron beam. This reduction of the current density results in a weakened magnetic field in the beam overlap region. The time-evolution of the counter-streaming beams and of the electric and magnetic fields, which result in their thermalization, depends on the nature of the instabilities and processes that are involved.

Previous related experiments have examined the simultaneous interaction of two or more laser pulses with a solid target. The laser pulses had intensities of $10^{14} - 10^{15}\text{W/cm}^2$ [17, 18]. In these experiments, the expansion of plasma bubbles at the front surface of the target was examined with the aim to study magnetic reconnection of the megagauss-fields, which encircle the individual plasmas and confine them. The moderate laser intensity has limited the particle flow speeds to the nonrelativistic regime. Such flows tend to thermalize electrostatically.

Here the speeds of the electron sheaths, which form before ion jets are launched, are relativistic and the magnetic fields sustained by their currents are confined to a narrow layer close to the surface. The instabilities that result in the thermalisation of the relativistic fast electron flows differ from the nonrelativistic ones in Ref. [17, 18] that involve electrons and ions.

The counter-streaming relativistic electrons give rise to a wide range of beam instabilities in this overlap layer. The potentially large number of instabilities can be re-

*Electronic mail: Mark.E.Dieckmann@itn.liu.se

duced to three, if we assume that only the electrons interact, that the thermal spread of the electron speeds is smaller than the difference of the mean speeds of both beams and that magnetic field effects in the beam overlap region are negligible. Negligible here means that the electron gyrofrequency is small compared to the growth rates of the instabilities. We obtain under these conditions the two-stream instability, the oblique mode instability and the filamentation or beam-Weibel instability. These instabilities are discussed in detail in Ref. [19]. Here we summarize their properties.

Let \mathbf{k} and \mathbf{v}_b be the wave vector of the growing waves and the difference vector between the mean velocities of the counter-streaming electron beams, respectively. Let α be the angle between \mathbf{k} and \mathbf{v}_b . The two-stream instability [20] is purely electrostatic for $\mathbf{k} \parallel \mathbf{v}_b$ ($\alpha = 0$). It saturates by the formation of electron phase space holes in the nonrelativistic [21] and relativistic regimes [19]. The coalescence instability [21] triggers the collapse of these nonlinear structures, which thermalizes the electron flow. What remains from the two counter-streaming electron beams is a single hot electron distribution with a low mean speed modulus. The net current is small and the magnetic field it drives is weak. The two-stream instability grows slower than the oblique mode instability if $|\mathbf{v}_b| \approx c$. The oblique modes have a mixed polarity and they are almost electrostatic. Their wave vectors \mathbf{k} form angles $0 < \alpha < 90^\circ$ with respect to \mathbf{v}_b and they become two-stream unstable modes if $\alpha = 0$. They also saturate by electron trapping [22]. Both instabilities thermalize the electrons electrostatically.

If the counter-streaming electron beams have a similar density and temperature and if they collide at a moderately relativistic speed, then both electrostatic instabilities are outgrown by the filamentation instability [23]. The latter is driven by the magnetic repulsion of electrons, which move into opposite directions. It saturates by magnetic trapping [24] and its final state are current channels, which contain charged particles that have the same current direction. These channels have a diameter of the order of the electron skin depth and are surrounded by strong magnetic fields. The plasma flow is eventually thermalized through the repeated mergers of the current channels. However, the magnetic fields remain strong in a broad spatial interval [25–28].

Our 2D PIC simulation, which uses the 2D3V code LAPINE [29], resolves a cross-section of the target that contains the surface normal. The electron flow at the rear surface is thus confined to a layer close to the one-dimensional surface with a width that is comparable to an electron skin depth. The colliding electron sheaths can drive two instabilities in this geometry. The two-stream instability, which results in electrostatic oscillations along the surface direction, and the filamentation instability, which separates both electron beams along the surface normal. Our simulation demonstrates that for the selected initial conditions the magnetic interaction is more important than the electrostatic one. A

laser-plasma experiment with similar initial conditions would thus allow us to drive the filamentation instability on the two-dimensional surface of the target. The experimentally measured data can be compared to the existing 2D and 3D simulation studies (See for example [25–28]) of colliding leptonic flows and test their validity. Studying this instability with a controlled laboratory experiment would provide us with a much needed better understanding of the magnetic field generation within gamma-ray burst (GRB) jets, which are spectacular releases of energetic electromagnetic radiation at cosmological distances [30]. A direct comparison of the filaments observed in a controlled laboratory experiment and those believed to exist close to the internal shocks of GRBs is possible if the plasma is collisionless, because then all observables can be scaled between both systems with the help of the electron plasma frequency [31].

This paper is structured as follows. Section 2 discusses the numerical scheme and the initial conditions. The results are presented in Section 3 and they are discussed in Section 4.

II. SIMULATION MODEL

Particle-in-cell simulation codes solve the numerical approximation of Maxwell's equations on a grid and they approximate the plasma by an ensemble of computational particles. The particle momenta are updated with the help of the relativistic Lorentz force equation. This simulation method is discussed in detail in Ref. [32]. We restrict our simulation to a 2D geometry.

Our initial and boundary conditions are as follows: Two equal laser pulses hit a thick plasma slab simultaneously and at normal incidence as depicted in Fig. 1. The target with a width of $110\lambda_0$ and thickness of $5\lambda_0$ is initially located between $z = 10\lambda_0$ and $15\lambda_0$, where $\lambda_0 = 1\mu\text{m}$ is the laser wavelength. The target consists of an initially charge-neutral mixture of electrons and Al^{10+} with mass $m_i = 27m_p$, where $m_p = 1836m_e$ is the proton mass. The initial density of the target is set to $50n_c$, where $n_c = 1.12 \times 10^{21}\text{cm}^{-3}$ is the critical density. The initial temperatures of the electrons and ions are both set to 1 keV for computational reasons. The simulation box size $L_z \times L_y = 30\lambda_0 \times 110\lambda_0$ is resolved by 1500×5500 cells, and the electrons and Aluminium ions are represented by 64 and 16 computational particles per cell, respectively. Two p -polarized laser pulses are incident normally from the left boundary and focused on the target at $y = \pm 30\lambda_0$, respectively. The midpoint between the laser pulses defines $y = 0$. The pulses rise up in the first $4T_0$ with a Gaussian profile and then maintain the peak intensity for $40T_0$, where $T_0 \sim 3.3$ fs is the laser cycle. The maximum intensity of the pulses is $5 \times 10^{19}\text{W}/\text{cm}^2$, corresponding to $a_0 = 6$. The laser pulses have a Gaussian spatial profile with a spot radius of $5\lambda_0$. The time step is $0.007T_0$. For both the transverse and longitudinal boundaries, absorbing boundary conditions are used for

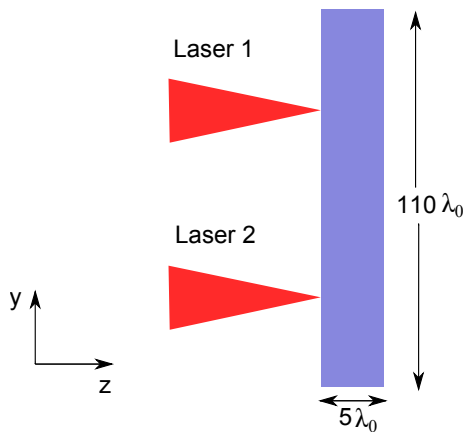


FIG. 1: (Color online) The simulation setup: The target (blue) has a thickness of $5\lambda_0$ along the z -direction and is located between $z = 10\lambda_0$ and $15\lambda_0$ in the simulation box. The target is hit by two equal laser pulses (red).

the fields and particles.

III. RESULTS

The impact of the double pulse generates two rarefaction waves, as can be seen in Fig. 2. The electrons are accelerated mainly by $\mathbf{J} \times \mathbf{B}$ heating (i.e., by the oscillating component of the laser's ponderomotive force) [33] to a temperature of ~ 1.0 MeV as the laser pulses irradiate the target, which is close to Haines' scaling $T_h = m_e c^2 (\sqrt{1 + \sqrt{2}a_0} - 1) = 1.01 \text{ MeV}$ [34] with a velocity of $0.95c$. The electron temperature obtained here is much lower than that given by ponderomotive scaling (~ 2.6 MeV) [35]. This discrepancy can be attributed to the fact that the electrons only interact with the laser pulse during a fraction of the laser period before being accelerated forward beyond the laser penetration region, due to that in our simulation that ultra-intense laser pulses irradiate an overdense target with a steep density interface. This situation is different from the mechanisms proposed by Kemp et al. [36] and May et al. [37]; a low density shelf is required for the former and the electron energy is gained in the vacuum from the transverse laser field in the latter case.

The hot electrons propagate through the target and form the two high energy density channels visible in Fig. 2(b) at $y = \pm 30\lambda_0$. A small part of the energetic electrons escape into the vacuum at the rear surface of the target. Their current, visualized in Fig. 2(a), is not balanced by an ion current and generates a strong sheath electromagnetic field, which reflects most of the hot electrons and confines them. The sheath field accelerates ions on the target's surface (See Fig. 2(c)), whose larger inertia implies that they trail the electrons in Fig. 2(d). The plasma density of both parabolic expanding rarefaction waves decreases with increasing distance from the target

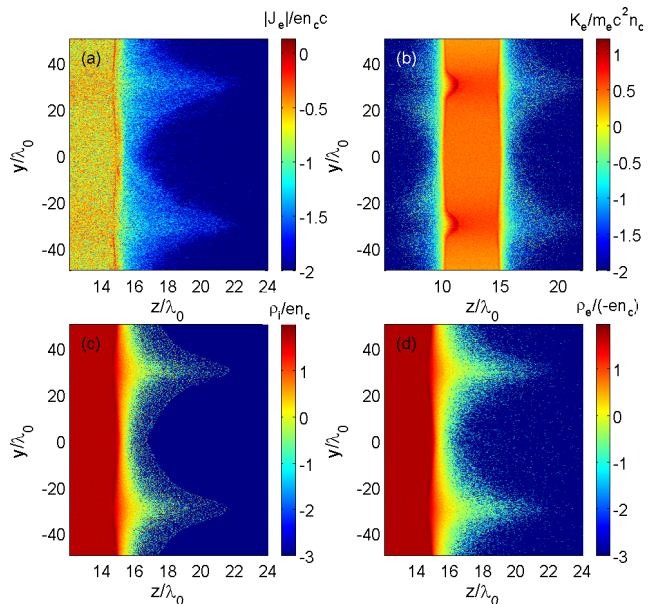


FIG. 2: (Color online) The amplitude of the electron current density ($|J_y + i*J_z|$) in the simulation plane (a), the electron kinetic energy density in units of $m_e c^2 n_e$ (b), the ion charge density in units of en_c (c) and the electron charge density in units of $-en_c$ (d). The amplitude of the current density is in units of $en_c c$. All color scales are 10-logarithmic and the simulation time is $t=120T_0$.

and the charge separation drives an ambipolar electric field.

The flow of hot electrons at the surface of the target and the return current, which flows within the target to provide current closure, result in the growth of magnetic fields orthogonal to the simulation plane, which is here the x -direction. In the case of a single laser pulse, strong surface magnetic fields will expand from the exit point of the electrons at the rear end of the target until they cover the surface uniformly. Here the currents driven by both laser pulses will eventually collide and a more complex magnetic topology is revealed by Fig. 3. The distribution of B_x at the early time $60T_0$ in Fig. 3(a), which is triggered by each laser pulse, equals that observed for single laser pulses. The hot electron's surface current sheaths expand at the speed $0.7c$, but they have not yet collided at $y = 0$. The polarity of B_x at $y = \pm 30\lambda_0$ switches, because the electrons above the interaction point flow in the opposite direction compared with those below that point.

The hot electron sheaths have collided at the time $102T_0$ in Fig. 3(b). The surface magnetic field has decreased in amplitude compared to that at $60T_0$ and the field is more confined along z . A sharp transition between the magnetic fields occurs at $y = 0$ and a localized magnetic structure is observed at $z \approx 15.5\lambda_0$ and $y \approx -4\lambda_0$. The polarity (negative amplitude) suggests that it is tied to the electron sheath generated by the upper laser pulse.

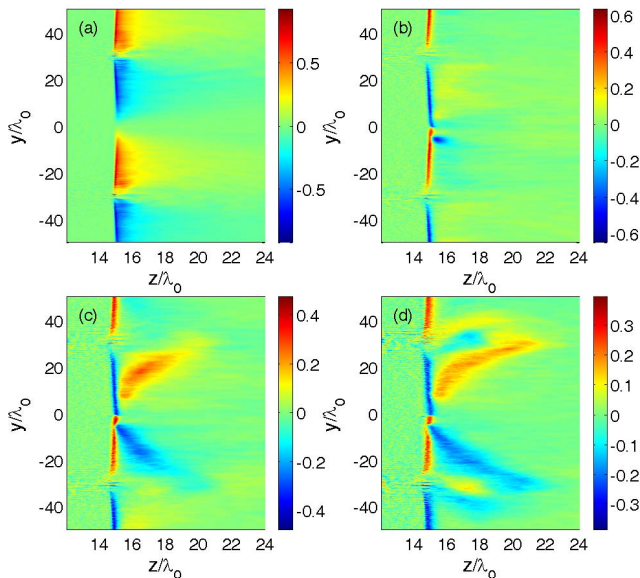


FIG. 3: (Color online.) Transverse magnetic field (B_x) distribution at $t=60T_0$ (a), $102T_0$ (b), $120T_0$ (c), and $140T_0$ (d), respectively. The amplitude is expressed in units of $m_e c \omega_0 / e$.

The current distribution is not perfectly symmetric at this time as we may expect from our symmetric simulation setup. However, the approximation of the plasma by computational particles introduces some randomness. Even a small difference of the current or charge density of the surface electrons can result in significant differences in the beam evolution, because their separation by the repulsive magnetic interaction corresponds to a plasma instability. Statistical variations could explain the observed asymmetric current distribution. Such differences do not limit the comparison of our PIC simulation results with that in experiments, since two identical laser pulses would never be obtained in experiments.

This current structure and the magnetic field it drives have expanded further in Fig. 3(c) ($t = 120T_0$). A second similar one has developed at $y > 0$ and $z > 15\lambda_0$. We call these structures magnetic wings. The distribution of B_x at the time $140T_0$ in Fig. 3(d) suggests that the currents responsible for the wings are about to reconnect to the surface currents at $|y| < 30\lambda_0$ and $z \approx 15\lambda_0$. We infer this from the magnetic field polarity. We find in Fig. 3(d) a magnetic field patch with a positive amplitude in the interval close to $y \approx 40\lambda_0$ and $z \approx 18\lambda_0$ and in an interval close to $y \approx 30\lambda_0$ and $z \approx 20\lambda_0$. Both are about to merge. Such a merger implies that the currents encircling both structures reconnect. An unambiguous demonstration of such a reconnection can only be provided by the electronic currents. They are, however, too noisy for this purpose. The magnetic field distribution is smoother, because it is connected to the well-resolved total current and not to the fluctuating current densities within individual simulation grid cells.

The magnetic fields observed in Fig. 3 are transient. The current, which has been driven directly by the laser pulses, will eventually be dissipated. The thermoelectric instability, an instability driven by a plasma density gradient that is not parallel to the temperature gradient [38], will eventually develop and remagnetize the plasma. The dynamics of the magnetic fields it drives and their reconnection have been examined in the experiments performed in Refs. [17, 18]. We do not consider them here.

Figure 4 displays J_y , which corresponds to the surface current along the initial target boundary, and the electric field's E_z component at two times (only the target's rear side is shown). The ambipolar E_z is tied to the density gradient of the rarefaction wave and it is here practically electrostatic. Strong surface currents are present in Fig. 4(a) at $z \approx 15\lambda_0$. The fluctuations observed for $z < 15\lambda_0$ are thermal noise. No such fluctuations are seen for $z > 15\lambda_0$, since the lower plasma density implies lower fluctuation amplitudes. The current filaments at $z \approx 15\lambda_0$ have a thickness, which is a few times the electron skin depth $c/\omega_p \approx 0.023\lambda_0$. Consider the point $y = 30\lambda_0$ in Fig. 4(a). The surface current above this point is negative, which implies that electrons move to increasing values of y . It has the opposite sign below. The hot surface electrons thus move away as expected from the point $y = 30\lambda_0$. In addition, a lower return current density at $z < 15\lambda_0$ is visible. Both currents encircle the surface magnetic field visible in Fig. 3(b).

The surface current in Fig. 4(a) maintains a practically constant strength from $|y| = 30\lambda_0$ up to $y = 0$. The electron flow has not been thermalized by an electrostatic instability, as this would demagnetize the flow around $y = 0$ and increase the electron temperature. The currents have been separated instead along the normal direction of the target's rear surface in a small y -interval close to $y \approx 0$. The surface current driven by the upper laser pulse is magnetically expelled at $y \approx -4\lambda_0$ and $z \approx 15.5\lambda_0$ and J_y reaches here a value $5.4 \times 10^{11} \text{ A/cm}^2$. The total current density is actually stronger, because the expelled current has J_y and J_z components due to its deflection along z . Its spatial correlation with the magnetic structure in Fig. 3(b) indicates that the expelled current drives it. The surface current driven by the lower laser pulse initially reconnects with the return current driven by the upper laser pulse. We attribute again the different behaviour of the electron flows driven by the upper and lower laser pulses to the break of symmetry by the plasma approximation by a finite number of computational particles and the resulting statistical variations. The symmetric wings in Fig. 3(c) evidence that both current sheaths get expelled at a later time. Note that we can not clearly associate a current with the overplotted contour lines of the wings in Fig. 4(b), because the current is too weak and noisy. The total current is, however, preserved since Fig. 3(c) clearly demonstrates that the peak amplitudes of the surface current and wing magnetic field are practically identical.

The reason for the widening of the expelled current

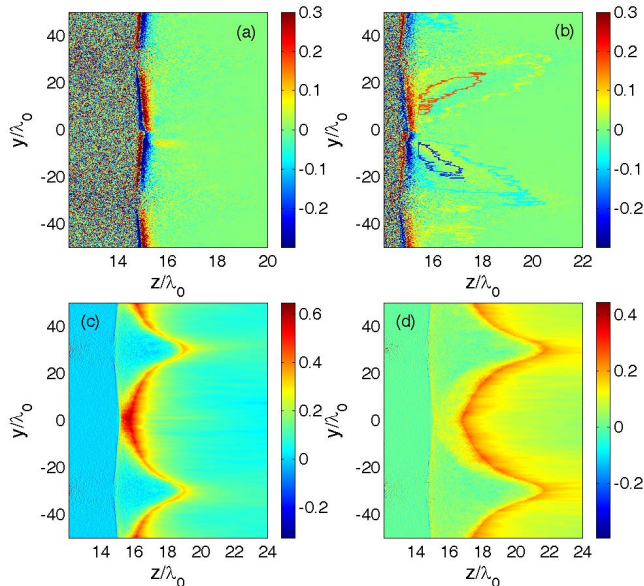


FIG. 4: (Color online.) The transverse current density (J_y) distribution at $t=102T_0$ is shown in (a) and that at $120T_0$ in (b). Several contour lines of B_x are overplotted in (b) using the same color scale as for the current density. The electric field (E_z) distribution at $t=90T_0$ is shown in (c) and that at $120T_0$ in (d). The color scale of the current density is restricted within $[-0.3, 0.3]$ in order to distinguish the current distribution clearly in the vacuum. The current density and the electric field amplitude are expressed in units en_{ec} and $m_e c \omega_0 / e$, respectively.

sheath, which is responsible for the spreading out of the magnetic wing with increasing distance from the target surface in Fig. 3(c), is given by Figs. 4(c) and 4(d). The parabolic ambipolar electric field visible in both plots outlines the front of the two rarefaction waves, which are driven by the laser pulses. This interpretation is supported by the electron and ion distributions in Figs. 2(c) and 2(d). Note that no ambipolar electric field can be observed at the original target boundary $z = 15\lambda_0$, because the strong surface magnetic field suppresses the electron mobility along the surface normal. A comparison between Fig. 3(c) and Fig. 4(d) demonstrates that the magnetic wings are located within the rarefaction wave. A current closure is thus achieved by the rarefaction wave's plasma. The plasma density within the rarefaction wave is below that of the solid target, which reduces the supported current density. The currents and the associated magnetic fields spread out in space.

It is interesting to know how the laser power and, thus, the characteristic speed of the electron sheath affect the interaction of the electrons and the magnetic fields in the sheaths' overlap layer. More specifically, we want to know if the filamentation instability could also be examined with weaker laser pulse intensities, like those used in the previous experiments [17, 18]. We have performed

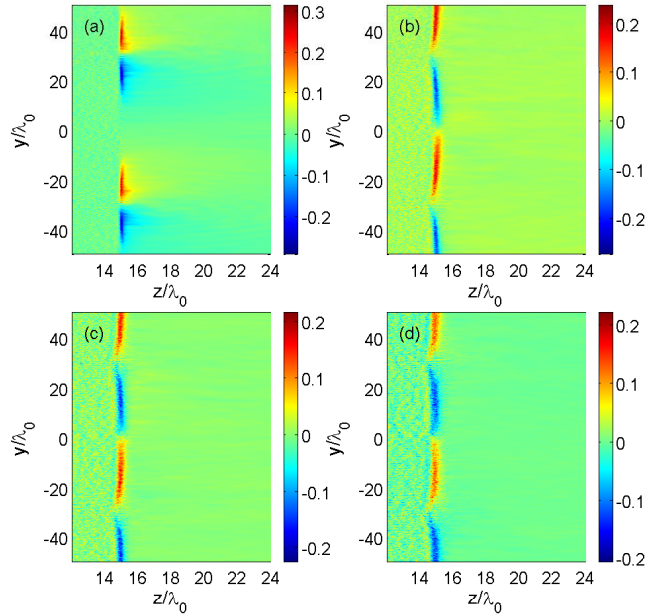


FIG. 5: (Color online.) Transverse magnetic field (B_x) distribution at $t=60T_0$ (a), $100T_0$ (b), $120T_0$ (c), and $140T_0$ (d), respectively, for the case with a laser intensity of $5 \times 10^{18} \text{W/cm}^2$. The other parameters are the same as that in Fig. 3

for this purpose a series of simulations with lower laser intensities, i.e., $I_0 = 5 \times 10^{16} \text{W/cm}^2$, $5 \times 10^{17} \text{W/cm}^2$, and $5 \times 10^{18} \text{W/cm}^2$, respectively. The magnetic field repulsion in the sheath overlap layer is not observed in any of the simulations. Figure 5 shows the evolution of the transverse magnetic field for the case study that employed a laser intensity $5 \times 10^{18} \text{W/cm}^2$. The magnetic field amplitude driven by the surface current is much weaker than that observed for a laser intensity $5 \times 10^{19} \text{W/cm}^2$ (Fig. 4). The maximum magnetic field here is $\sim 2.8 \times 10^7 \text{Gauss}$ at $t = 100T_0$, only one third of the latter ($\sim 7.4 \times 10^7 \text{Gauss}$). Both the current density and the expansion speed of the electron current along the surface here ($\sim 0.4c$) are much smaller than that of the latter. Most importantly, Fig. 5 reveals a different magnetic topology close to $y \approx 0$ compared to Fig. 3. The electrons from both sheaths do not interpenetrate in the simulation that uses the weaker laser pulse. This implies that the driving currents are closed by the return current within the target. A magnetic distribution develops at the surface, which is stationary during the resolved time interval. The absence of counter-streaming electron beams implies that no filamentation instability can develop here. If the electron beams would interpenetrate close to $y \approx 0$, their nonrelativistic speeds $\approx 0.4c$ observed in the simulation would probably result in a thermalization through the quasi-electrostatic two-stream and oblique modes [23].

IV. CONCLUSION

In summary, we have examined the plasma processes triggered by the impact of a laser double-pulse on a solid target, using PIC simulations. The large 2D simulation box has resolved a cross section of the target. Each laser pulse has accelerated the electrons to relativistic speeds. The electrons have mainly been accelerated along the propagation direction of the laser pulse and they have crossed the target. The electrons re-emerged on the target's rear surface, where they have been deflected by the self-generated ambipolar electrostatic field. They have expanded along the target's surface and they have collided at the midpoint between the laser axes. The plasma did not thermalize electrostatically when the electron sheaths collided. Their relativistic speeds resulted in a dominant magnetic rather than electrostatic interaction. Our 2D geometry implied that the current sheaths were expelled from the target by their mutual interaction and moved into the rarefaction wave, provided that the driving laser pulse is ultra-intense. The resolution of a second dimension of the target's surface by a currently too expensive 3D PIC simulation would allow for stud-

ies of the filamentation instability [19, 25, 30] within the overlap layer of the colliding electron sheaths. Our simulation results thus suggest that this instability, which is thought to magnetize energetic astrophysical flows, can be observed in a laboratory experiment provided that the laser pulse is ultra-intense and the electron flow speeds are relativistic.

Acknowledgments

This work was supported by EPSRC (Grant No. EP/D06337X/1) and partly supported in the framework of the HiPER consortium. M.B. also acknowledges funding from projects ELI (Grant No. CZ.1.05/1.1.00/483/02.0061) and OPVK 3 (Grant No. CZ.1.07/2.3.00/20.0279). X.H.Y. acknowledges the support from the China Scholarship Council, the NSFC (Grant Nos. 10975185 and 10976031), the Innovation Foundation for Postgraduate of Hunan Province (Grant No. CX2010B008) and NUDT (Grant No. B100204). G.S. wishes to acknowledge the Leverhulme Trust (Grant No. ECF-2011-383).

-
- [1] T. Nakamura, S. Kato, H. Nagatomo, and K. Mima, *Phys. Rev. Lett.* **93**, 265002 (2004).
- [2] Y. T. Li, X. H. Yuan, M. H. Xu, Z. Y. Zheng, Z. M. Sheng, M. Chen, Y. Y. Ma, W. X. Liang, Q. Z. Yu, Y. Zhang, F. Liu, Z. H. Wang, Z. Y. Wei, W. Zhao, Z. Jin, and J. Zhang, *Phys. Rev. Lett.* **96**, 165003 (2006).
- [3] X. H. Yang, H. Xu, Y. Y. Ma, F. Q. Shao, Y. Yin, H. B. Zhuo, M. Y. Yu, and C. L. Tian, *Phys. Plasmas* **18**, 023109 (2011).
- [4] M. Borghesi, J. Fuchs, S. V. Bulanov, A. J. Mackinnon, P. K. Patel, and M. Roth, *Fusion Sci. Technol.* **49**, 412 (2006).
- [5] T. Toncian, M. Borghesi, J. Fuchs, E. d'Humières, P. Antici, P. Audebert, E. Brambrink, C. A. Cecchetti, A. Pipahl, L. Romagnani, and O. Willi, *Science* **312**, 410 (2006).
- [6] M. Tabak, J. Hammer, M. E. Glinsky, W. L. Kruer, S. C. Wilks, J. Woodworth, E. M. Campbell, M. D. Perry, and R. J. Mason, *Phys. Plasmas* **1**, 1626 (1994).
- [7] G. Sarri, A. Macchi, C. A. Cecchetti, S. Kar, T. V. Liseykina, X. H. Yang, M. E. Dieckmann, J. Fuchs, M. Galimberti, L. A. Gizzi, R. Jung, I. Kourakis, J. Osterholz, F. Pegoraro, A. P. L. Robinson, L. Romagnani, O. Willi, and M. Borghesi, *Phys. Rev. Lett.*, in press.
- [8] L. Romagnani, J. Fuchs, M. Borghesi, P. Antici, P. Audebert, F. Ceccherini, T. Cowan, T. Grismayer, S. Kar, A. Macchi, P. Mora, G. Pretzler, A. Schiavi, T. Toncian, and O. Willi, *Phys. Rev. Lett.* **95**, 195001 (2005).
- [9] X. H. Yang, Y. Y. Ma, F. Q. Shao, H. Xu, M. Y. Yu, Y. Q. Gu, T. P. Yu, Y. Yin, C. L. Tian, and S. Kawata, *Laser Part. Beams* **28**, 319 (2010).
- [10] M. Borghesi, L. Romagnani, A. Schiavi, D. H. Campbell, M. G. Haines, O. Willi, A. J. Mackinnon, M. Galimberti, L. Gizzi, R. J. Clarke, and S. Hawkes, *Appl. Phys. Lett.* **82**, 1529 (2003).
- [11] K. Quinn, P. A. Wilson, B. Ramakrishna, G. Sarri, L. Romagnani, A. Pipahl, O. Willi, L. Lancia, J. Fuchs, D. C. Carroll, M. N. Quinn, P. Gallegos, X. H. Yuan, P. McKenna, R. J. Clarke, D. Neely, M. Notley, A. Macchi, and M. Borghesi, *Eur. Phys. J. D* **55**, 293 (2009).
- [12] R. Kodama, Y. Sentoku, Z. L. Chen, G. R. Kumar, S. P. Hatchett, Y. Toyama, T. E. Cowan, R. R. Freeman, J. Fuchs, Y. Izawa, M. H. Key, Y. Kitagawa, K. Kondo, T. Matsuoka, H. Nakamura, M. Nakatsutsumi, P. A. Norreys, T. Norimatsu, R. A. Snavely, R. B. Stephens, M. Tampo, K. A. Tanaka, and T. Yabuuchi, *Nature (London)* **432**, 1005 (2004).
- [13] Y. Sentoku, K. Mima, H. Ruhl, Y. Toyama, R. Kodama, and T. E. Cowan, *Phys. Plasmas* **11**, 3083 (2004).
- [14] T. Nakamura, K. Mima, H. Sakagami, and T. Johzaki, *Phys. Plasmas* **14**, 053112 (2007).
- [15] P. McKenna, D. C. Carroll, R. J. Clarke, R. G. Evans, K. W. D. Ledingham, F. Lindau, O. Lundh, T. McCanny, D. Neely, A. P. L. Robinson, L. Robson, P. T. Simpson, C. G. Wahlström, and M. Zepf, *Phys. Rev. Lett.* **98**, 145001 (2007).
- [16] K. Quinn, P. A. Wilson, C. A. Cecchetti, B. Ramakrishna, L. Romagnani, G. Sarri, L. Lancia, J. Fuchs, A. Pipahl, T. Toncian, O. Willi, R. J. Clarke, D. Neely, M. Notley, P. Gallegos, D. C. Carroll, M. N. Quinn, X. H. Yuan, P. McKenna, T. V. Liseykina, A. Macchi, and M. Borghesi, *Phys. Rev. Lett.* **102**, 194801 (2009).
- [17] P. M. Nilson, L. Willingale, M. C. Kaluzas, C. Kamperidis, S. Minardi, M. S. Wei, P. Fernandes, M. Notley, S. Bandyopadhyay, M. Sherlock, R. J. Kingham, M. Tatarakis, Z. Najmudin, W. Rozmus, R. G. Evans, M. G. Haines, A. E. Dangor, and K. Krushelnick, *Phys. Rev. Lett.* **97**, 255001 (2006).

- [18] C. K. Li, F. H. Séguin, J. A. Frenje, J. R. Rygg, R. D. Petrasso, R. P. J. Town, O. L. Landen, J. P. Knauer and V. A. Smalyuk, *Phys. Rev. Lett.* **99**, 055001 (2007).
- [19] A. Bret, L. Gremillet, and M. E. Dieckmann, *Phys. Plasmas* **17**, 120501 (2010).
- [20] L. E. Thode, and R. N. Sudan, *Phys. Rev. Lett.* **30**, 732 (1973).
- [21] H. L. Roberts, and K. V. Berk, *Phys. Rev. Lett.* **19**, 297 (1967).
- [22] M. E. Dieckmann, J. T. Frederiksen, A. Bret, and P. K. Shukla, *Phys. Plasmas* **13** 112110 (2006).
- [23] A. Bret, L. Gremillet, and J. C. Bellido, *Phys. Plasmas* **14**, 032103 (2007).
- [24] R. C. Davidson, D. A. Hammer, I. Haber, and C. E. Wagner, *Phys. Fluids* **15**, 317 (1972).
- [25] Y. Kazimura, J. I. Sakai, T. Neubert, and S. V. Bulanov, *Astrophys. J.* **498**, L183 (1998).
- [26] L. O. Silva, R. A. Fonseca, J. W. Tonge, J. M. Dawson, W. B. Mori, and M. V. Medvedev, *Astrophys. J.* **596**, L121 (2003).
- [27] K. I. Nishikawa, J. Niemiec, P. E. Hardee, M. Medvedev, H. Sol, Y. Mizuno, B. Zhang, M. Pohl, M. Oka, and D. H. Hartmann, *Astrophys. J.* **698**, L10 (2009).
- [28] G. C. Murphy, M. E. Dieckmann, and L. O. Drury, *Int. J. Mod. Phys. D* **19**, 707 (2010).
- [29] H. Xu, W. W. Chang, and H. B. Zhuo, *Chin. J. Comput. Phys.* **19**, 305 (2002). (in Chinese)
- [30] M. V. Medvedev, and A. Loeb, *Astrophys. J.* **526**, 697 (1999).
- [31] M. Honda, J. Meyer-ter-Vehn, and A. Pukhov, *Phys. Plasmas* **7**, 1302 (2000).
- [32] J. M. Dawson, *Rev. Mod. Phys.* **55**, 403 (1983).
- [33] W. L. Kruer and K. Estabrook, *Phys. Fluids* **28**, 430 (1985).
- [34] M. G. Haines, M. S. Wei, F. N. Beg, and R. B. Stephens, *Phys. Rev. Lett.* **102**, 045008 (2009).
- [35] S. C. Wilks, W. L. Kruer, M. Tabak, and A. B. Langdon, *Phys. Rev. Lett.* **69**, 1383 (1992).
- [36] A. J. Kemp, Y. Sentoku, and M. Tabak, *Phys. Rev. E* **79**, 066406 (2009).
- [37] J. May, J. Tonge, F. Fiuza, R. A. Fonseca, L. O. Silva, C. Ren, and W. B. Mori, *Phys. Rev. E* **84**, 025401 (2011).
- [38] D. A. Tidman, and L. L. Burton, *Phys. Rev. Lett.* **37**, 1397 (1976).